Nuclear Instruments and Methods in Physics Research A 610 (2009) 164–168

Contents lists available at ScienceDirect

Nuclear Instruments and Methods in Physics Research A

journal homepage: www.elsevier.com/locate/nima

Development of gaseous PMT with micropattern gas detector

Fuyuki Tokanai [a,*], Takayuki Sumiyoshi [b], Hiroyuki Sugiyama [c], Teruyuki Okada [c], Noboru Ohishi [c], Takayuki Ohmura [c], Hirohisa Sakurai [a], Shuichi Gunji [a]

[a] Department of Physics, Yamagata University, Yamagata 990-8560, Japan
[b] Department of Physics, Tokyo Metropolitan University, Tokyo 192-0397, Japan
[c] Electron Tube Division, Hamamatsu Photonics K.K., Shizuoka 438-0193, Japan

ARTICLE INFO

Available online 23 May 2009

Keywords:
Gaseous PMT
Glass capillary plate
Micropattern gas detector

ABSTRACT

We have developed gaseous photomultiplier tubes (PMTs) with a bialkali photocathode, combined with micropattern gas detectors (MPGDs) such as a glass capillary plate (CP), a gas electron multiplier (GEM) and a Micromegas detector. Gaseous PMTs with two different gas mixtures of Ar (90%)+CH_4 (10%) and Ne (90%)+CF_4 (10%) were investigated at a gas pressure of 1 atm. Quantum efficiencies of up to 12% were obtained for both neon and argon gas mixtures. A new glass CP made of Pyrex glass has been developed for a hole-type MPGD. The glass is well-suited for high-level cleanliness and reaction conditions required for the production of bialkali photocathodes. A gain of up to 1.5×10^4 and an energy resolution of 23% were obtained for 5.9 keV X-rays. This latest result and the basic performance of the gaseous PMTs are described.

1. Introduction

In the last few years, considerable effort has been devoted to the development of gaseous photomultiplier tubes (PMTs) with a micropattern gas detector (MPGD) sensitive to light in the region ranging from vacuum ultraviolet (VUV) to infrared (IR) wavelengths (see Refs. [1–7] and references therein). The potential advantage of the gaseous PMT is that it can achieve a very large effective area with moderate position and timing resolutions. In addition, it can be easily operated under a very high magnetic field compared with the conventional vacuum-based PMT. In the VUV range, a ring imaging Cherenkov detector (RICH), which consists of a cesium iodide (CsI) photocathode coupled to a multiwire proportional chamber (MWPC), has been successfully and widely utilized in the field of high-energy physics for particle identification (see Refs. [8,9] and references therein). However, it has been suggested that the open geometry of the MWPC limits the sensitivity and lifetime of the CsI photocathode due to both photon and ion feedback [8]; almost all the photons and ions produced during electron multiplication reach the photocathode, where they cause secondary and successive avalanches by interacting with the photocathode. Therefore, the maximum achievable gain is limited to approximately 10^5 due to the feedbacks from the interaction of the MWPCs with the CsI photocathodes [8].

Concerning gaseous PMTs that are sensitive to visible light, the effect of the feedback is more serious because the work function of the bialkali is lower than that of the CsI photocathode [3]. It is expected that the photon and ion feedbacks cause faster degradation of the bialkali photocathode than that of the CsI photocathode. Hence, the maximum achievable gain is limited to approximately 100 due to the feedback [10]. Several recent developments have been achieved using hole-type MPGDs such as the gas electron multiplier (GEM) [11] and glass capillary plate (CP) [12] to satisfy the demand for higher sensitivity and long-term photon detector [1–3,5–7]. Attempts to develop MPGDs with a CsI photocathode seem to be feasible since the geometry of the hole-type MPGDs plays the role of both masking photons and absorbing ions [7,13]. However, to develop a gaseous PMT with a bialkali photocathode, attention must also be paid to the high chemical activity of the bialkali metal. Thus, the selection of the material of the MPGD is crucial; in particular, the material should be well-suited to high-level cleanliness and reaction conditions required for the production of bialkali photocathodes. To evaluate the MPGD in a gaseous PMT sensitive to visible light, we have investigated the characteristics of sealed gaseous PMTs with a bialkali photocathode combined with MPGDs such as glass CP, GEM and Micromegas detector [14]. In this paper, we describe the basic performance of gaseous PMTs, particularly the production of the photocathode, quantum efficiency, gain and photon and ion feedback.

2. Basic properties of gaseous PMTs

2.1. Quantum efficiency in gas mixtures

To begin the first study on the production of a bialkali photocathode, we constructed a double Micromegas detector in

* Corresponding author. Tel.: +81 23 628 4554; fax: +81 23 628 4567.
E-mail address: tokanai@sci.kj.yamagata-u.ac.jp (F. Tokanai).

0168-9002/$ - see front matter © 2009 Elsevier B.V. All rights reserved.
doi:10.1016/j.nima.2009.05.111

a gaseous PMT following the previous work [15]. A photograph and schematic view of the double Micromegas detector with a bialkali photocathode are shown in Fig. 1. The glass vessel, electrode and insulator are the same as those used in the vacuum-type PMT developed at Hamamatsu Photonics K.K. Each Micromegas detector is made of Ni mesh with square holes of 43 μm × 43 μm with 78 μm mesh spacing. The space between the first and second mesh is 600 μm, and that between the second mesh and the anode plate is 500 μm. The fabrication of the bialkali photocathode (K–Cs–Sb) was performed at Hamamatsu Photonics K.K. by the same process used to produce the conventional vacuum-type PMT.

The gaseous PMT was filled with Ar (90%)+CH_4 (10%) or Ne (90%)+CF_4 (10%) gas mixtures at 1 atm. The photocathode was irradiated with photons from a tungsten lamp at the temperature of 2856 K (black-body radiation) and the luminous flux ranging from 10^{-5} to 10^{-9} lm. The quantum efficiency (QE) was determined by measuring the photoelectron currents using current meters at the photocathode ($I_{cathode}$) and the first mesh (I_{mesh1}) as shown in Fig. 1(b).

The QEs of the gaseous PMT with a bialkali photocathode are shown in Fig. 2 as a function of wavelength for the gas mixtures of Ar (90%)+CH_4 (10%) and Ne (90%)+CF_4 (10%). The electric field at the collection area between the photocathode and the first mesh was set to 150 V/cm for the QE measurements. The QE for the neon gas mixture is similar to that for the argon gas mixture. The maximum QEs are 14% and 12% for the neon and argon mixtures at wavelengths 350 and 420 nm, respectively. The QEs of the same PMT in a vacuum environment are also shown in Fig. 3 before and after filling the argon gas mixture. The QE in the evacuated PMT was approximately 20% before the gas filling at wavelengths between 300 and 500 nm. The deterioration of QE after filling the gas can be explained by the effect of photoelectron backscattering due to collisions with the gas molecules. Although the QE was degraded to approximately 12% upon filling the gas, it recovered its original value when the gas was evacuated again. Moreover, there was no deterioration of the QE over one and a half years for the sealed gaseous PMT filled with the argon gas mixture. From these results, it is confirmed that there is no degradation of the bialkali photocathode resulting from the inefficient sealing of the glass vessel and the escape of gas from the PMT.

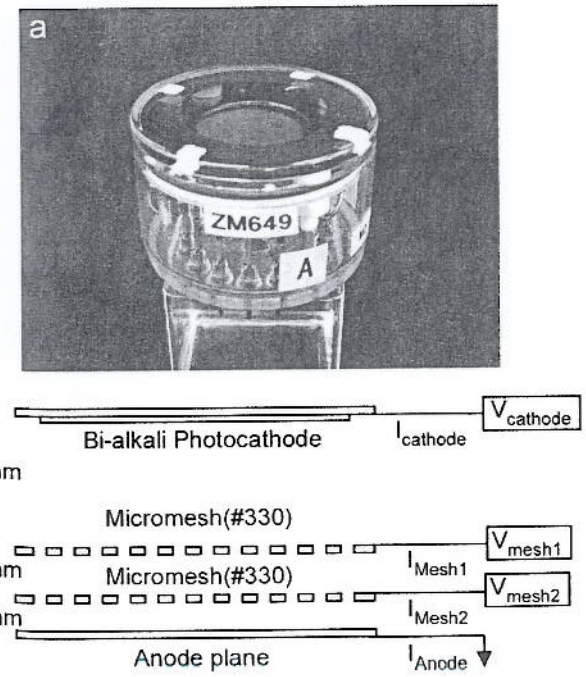

Fig. 1. Photograph (a) and schematic view (b) of the sealed gaseous PMT with a bialkali photocathode and double Micromegas detector.

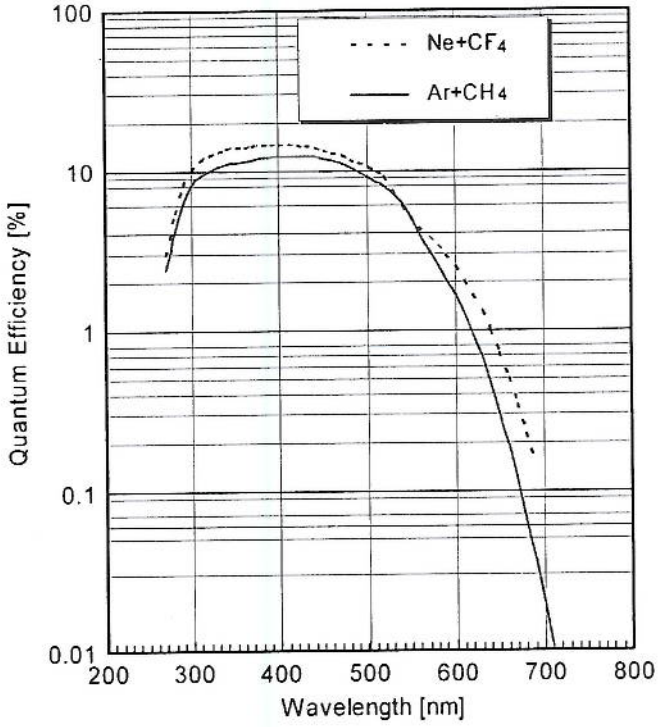

Fig. 2. Quantum efficiencies of the sealed gaseous PMT with a bialkali photocathode and double Micromegas detector for the gas mixtures of Ar (90%)+CH_4 (10%) and Ne (90%)+CF_4 (10%) at 1 atm as a function of wavelength.

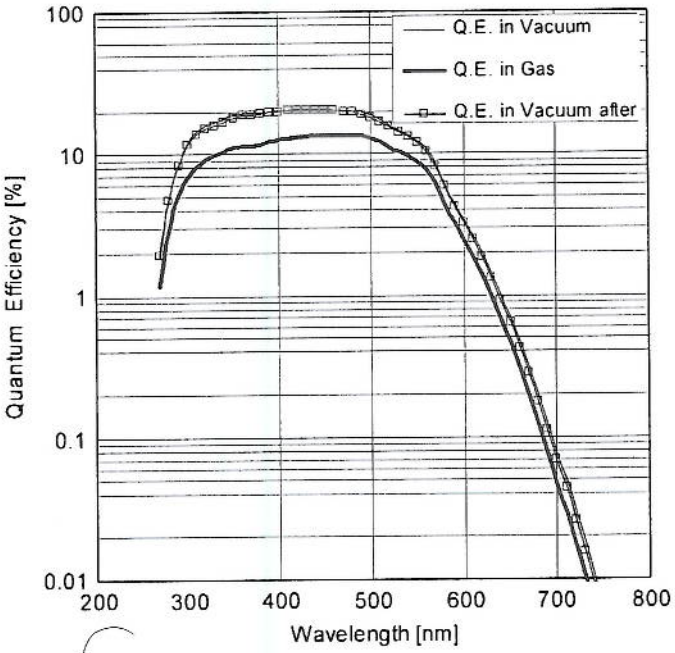

Fig. 3. Quantum efficiencies of the gaseous PMT with a bialkali photocathode and double Micromegas detector measured in vacuum before and after filling the argon gas mixtures. The maximum QE in the evacuated PMT is approximately 20% at wavelengths between 300 and 500 nm. The QE of the sealed gaseous PMT for Ar (90%)+CH_4 (10%) at 1 atm is indicated as a solid thick line (blue).

2.2. Gain of the gaseous PMT with double micromegas detector

The gain of the gaseous PMT with the double Micromegas detector was studied by measuring the signal currents at the anode (I_{anode}), first mesh (I_{mesh1}), second mesh (I_{mesh2}) and the photocathode ($I_{cathode}$) while varying the applied voltage of the first and second meshes. The voltage between the first and second mesh is fixed from the difference in voltage (ΔV_{mesh}) between the second mesh and the anode. The electric field between the photocathode and the first mesh is kept at 170 V/cm. Fig. 4 shows the dependence of the signal currents on ΔV_{mesh} above 450 V. The current at the photocathode is less than 0.1 nA throughout the entire measurement. It is clear that almost all the ions produced at the double Micromegas are collected by both the meshes. The ion feedback, defined as the ratio of $I_{cathode}$ to I_{anode}, is estimated to be less than 2.5×10^{-3} when $\Delta V_{mesh} = 495$ V. This value is about 100 times larger than that required for the practical application of single photoelectron detection.

The gain of the gaseous PMT was obtained by measuring the ratio of I_{anode} to $I_{cathode}$ ($\Delta V_{mesh} = 0$ V). Fig. 5 shows the gain as a function of the applied voltage (ΔV_{mesh}) for the Micromegas detector; the gain reached 2×10^3 without a large deviation from the exponential curve, indicating photon and ion feedbacks [16]. However, unexpected signals resulting from the operation of the double-mesh structure appear at a gain above 2×10^3 for the neon gas mixture. This secondary effect was also observed in the previous measurement with a gas mixture of Ar (90%)+CH_4 (10%) at a gain of approximately 6×10^3 [15]. Therefore, we concluded that it is not appropriate to apply the gaseous PMT with the double Micromegas detector to a single-photon detector, for which a gain of over 5×10^5 is necessary for practical operation. Thus, we started to develop a gaseous PMT with a bialkali photocathode using the combination of a hole-type MPGD and a Micromegas on the basis of previous works [7,15].

3. Evaluation of bialkali photocathode for gaseous PMT with hole-type MPGD

3.1. Material of the hole-type MPGD

As the bialkali photocathode is chemically very unstable, the materials inside the PMT must satisfy the high level of cleanliness required for the production of a bialkali photocathode. At present,

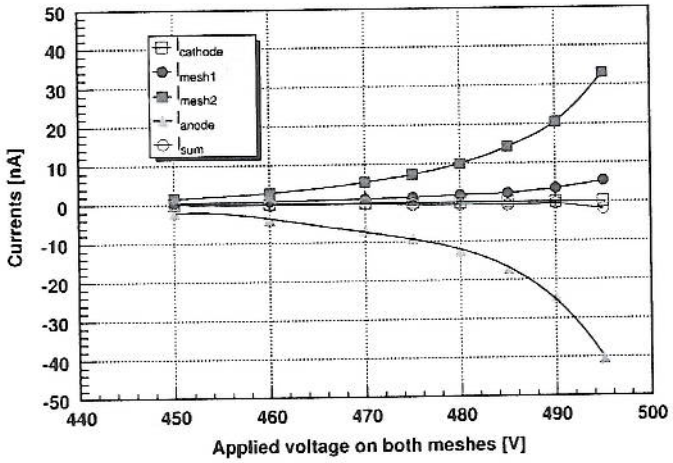

Fig. 4. Electrode currents ($I_{cathode}$, I_{mesh1}, I_{mesh2}, I_{anode} and their sum) of the sealed gaseous PMT with a bialkali photocathode and double Micromegas detector as a function of ΔV_{mesh} between the second mesh and the anode. The filled gas is Ne (90%)+CF_4 (10%) at 1 atm.

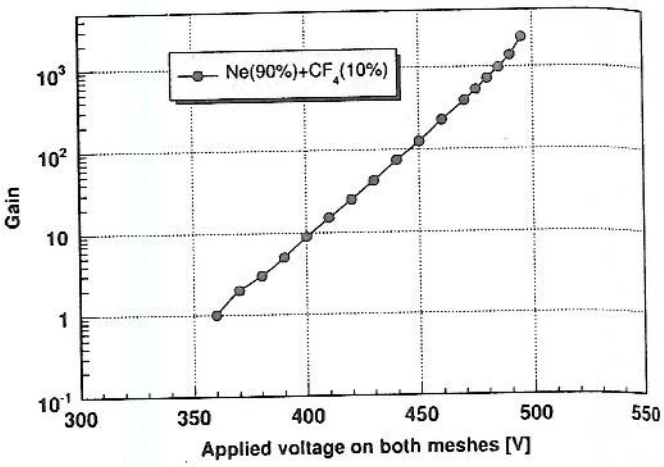

Fig. 5. Gain of the sealed gaseous PMT with a bialkali photocathode and double Micromegas detector for Ne (90%)+CF_4 (10%) at 1 atm as a function of ΔV_{mesh}.

the main materials of hole-type MPGDs are Kapton and lead glass, which are used as the substrates for GEM and glass CP, respectively. Using these materials, we attempted to fabricate gaseous PMTs with a bialkali photocathode combined with the hole-type MPGD. We tested two types of hole-type MPGDs having different substrates: a glass CP made of lead glass and a GEM made of Kapton (Kapton GEM). The other materials and parts as well as the configuration of the gaseous PMTs are identical to those used for the measurement by the double Micromegas detector except for the first mesh. The CP has a thickness of 0.4 mm and an individual capillary diameter of 100 μm. The hole diameter and the hexagonal array pitch of GEM are 70 and 140 μm, and the thickness is 50 μm.

3.2. Fabrication of bialkali photocathode

The fabrication of the bialkali photocathode (K–Cs–Sb) was performed by the process used for the production of the gaseous PMT with a double Micromegas detector; a thin layer of Sb is deposited on a substrate of Koval glass and is activated by bialkali metals (K–Cs). First we observed the colors of the surface on Koval glass after fabricating the bialkali photocathode. For the glass CP, the surface was light brown, similar to that of vacuum-type PMT. In contrast, it was colorless for the Kapton GEM. These results imply that the bialkali K–Cs vapor reacts with the material of the GEM. We performed an additional experiment to investigate the chemical reaction. A piece of Kapton was set in glass ampoules filled with the bialkali K–Cs or K vapor. After a while, the color of Kapton gradually changed to grey as K evaporated then to dark brown as soon as Cs started to evaporate. These changes in the color are attributed to an absorption reaction between the bialkali metals and the organic material in the GEM.

The photocathode sensitivity S_k, defined as the ratio of the cathode current $I_{cathode}$ to the incident flux (Φ), was measured to investigate the quality of the production of the bialkali photocathode. The photocathode was illuminated with focused visible light from a tungsten lamp. S_k was 56.3 μA/lm for the gaseous PMT with the glass CP, which is consistent with that for the gaseous PMT with a double Micromegas detector. S_k was 1.5 μA/lm for the gaseous PMT with the Kapton GEM, which is less than 3% of that of the glass CP. The experimental results clearly show that the material of the GEM chemically reacts with the bialkali metals and affects the production of the bialkali photocathode on the substrate of the Koval glass.

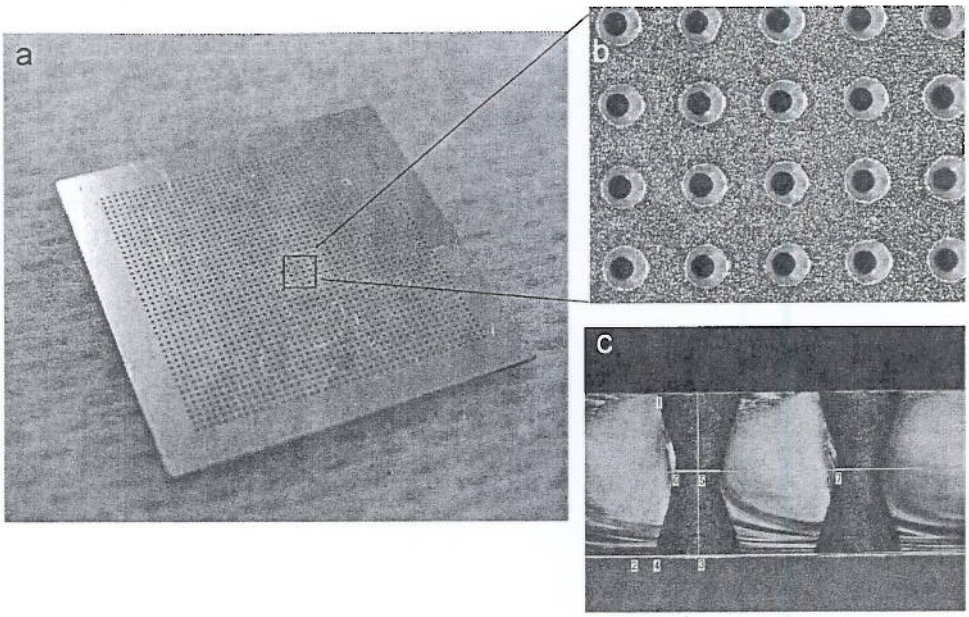

Fig. 6. Photograph of the Pyrex glass CP (a), a micrograph (b) and a scanning electron microscope image of the cross-section of the glass plate (c). The thickness of the CP is 300 μm, and the diameter and pitch of each capillary are 160 and 300 μm, respectively. Each hole has a double-conical shape with 124 μm diameter at the centre of the glass.

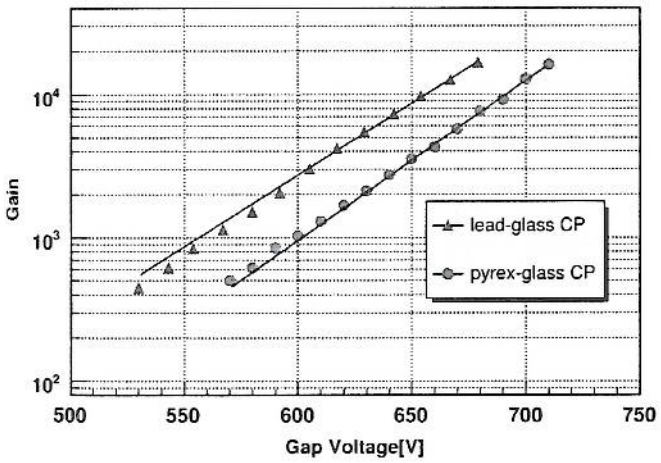

Fig. 7. Gain as a function of the voltage across the Pyrex glass CP electrodes for Ne (90%)+CF4 (10%) gas mixture at 1 atm obtained with 5.9 keV X-rays. The gain for the lead glass CP with a thickness of 400 μm and a hole diameter of 100 μm is indicated for comparison.

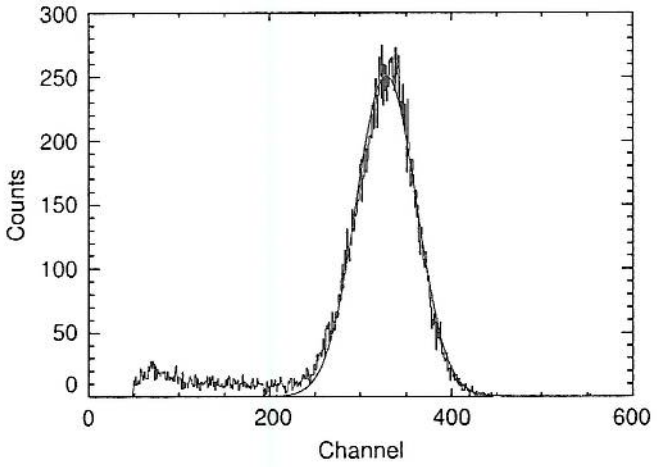

Fig. 8. Pulse height distribution of the charge signal of the Pyrex glass CP gas detector for a collimated ^{55}Fe source. The energy resolution is 23% (FWHM) for 5.9 keV X-rays.

3.3. *Pyrex glass capillary plate*

In contrast, the production of the bialkali photocathode seems to be problem-free for the PMT with the lead glass CP. However, our experiment shows that the conductivity on the surface of the wall of the lead glass changed after the production of the bialkali photocathode. This result indicates that a chemical reaction between the lead glass and the bialkali metal occurs at the surface of the wall. Indeed, the photoelectrons cannot enter the electron multiplication region in the CP, since the penetration of the bialkali metal causes the deterioration of the electric field in the drift region. Therefore, we started developing a hole-type MPGD with Pyrex glass that allows the problem-free production of bialkali photocathode. A micrograph of the Pyrex glass CP is shown in Fig. 6. Its thickness is 300 μm, and the diameter and pitch of each capillary are 160 and 300 μm, respectively. The electrodes are made of Al fabricated onto the two flat surfaces of a plate. Each hole has a double-conical shape with 124 μm diameter at the centre of the glass.

Basic performance tests of the Pyrex CP gas detector were carried out with an X-ray source using the experimental setup described in Ref. [17]. Fig. 7 shows the gain for the Ne (90%)+CF_4 (10%) gas mixture as a function of the voltage across the glass CP electrodes. The gain was obtained by measuring the amplitude of the charge output from the CP anode using a digital oscilloscope. Gains of up to 1.5×10^4 were safely achieved using a single CP. The gain obtained with the lead glass CP with thickness and hole diameter of 400 and 100 μm, respectively, is also indicated for comparison. At the same gas gain, the operating voltage for the Pyrex glass CP was ~80 V higher than that for the lead glass CP. The typical pulse height spectrum for 5.9 keV X-rays is shown in Fig. 8. The energy resolution is 23%, which agrees with the result obtained using the lead glass CP gas detector [17]. Following the successful operation of the Pyrex glass CP upon X-ray irradiation,

we are currently developing the gaseous PMT with bialkali photocathode.

4. Summary and discussion

The potential advantages of the gaseous PMT are very large effective area with moderate position and timing resolutions. It can also be easily operated under a very high magnetic field, compared to conventional vacuum-based PMT. The characteristics are important in experiments in elementary particle physics using accelerators and in clinical applications using a combination of positron emission tomography (PET) and magnetic resonance imaging (MRI). To develop a gaseous PMT, we have investigated the basic characteristics of gaseous PMTs with a bialkali photocathode combined with MPGDs with a glass CP, a GEM, and a Micromegas detector.

Quantum efficiencies of up to 12% were obtained for the gaseous PMT with a bialkali photocathode filled with neon and argon gas mixtures. Although these efficiencies were lower than that in vacuum due to photoelectron backscattering, there was no deterioration of efficiency over more than one and a half years for the gas within the sealed glass vessel. From the investigation of the production of the bialkali photocathode in gaseous PMT, we found that Pyrex glass is a more suitable material as a hole-type MPGD than other materials such as lead glass and Kapton. The Pyrex glass CP gas detector was operated with a gas mixture of Ne (90%)+CF_4 (10%) at 1 atm. We successfully obtained a gain of up to 1.5×10^4 and an energy resolution of 23% for 5.9 keV X-rays. A high gain of above 5×10^5 is required for practical applications including single-photoelectron imaging. To satisfy this requirement, the development of a gaseous PMT with cascaded MPGD is under way.

Acknowledgements

We would like to thank J. Va'vra for helpful discussions and suggestions about the gaseous PMT. This work was supported in part by a JSPS Grant-in-Aid.

References

[1] V. Peskov, et al., Nucl. Instr. and Meth. A 433 (1999) 492.
[2] A. Breskin, et al., Nucl. Instr. and Meth. A 433 (2000) 58.
[3] T. Francke, et al., IEEE Trans. Nucl. Sci. NS-49 (2002) 977 (and references therein).
[4] J. Derre, Y. Giomataris, Nucl. Instr. and Meth. A 477 (2002) 23 (and references therein).
[5] R. Chechik, et al., Nucl. Instr. and Meth. A 502 (2003) 195 (and references therein).
[6] J. Va'vra, T. Sumiyoshi, Nucl. Instr. and Meth. A 535 (2004) 334 (and references therein).
[7] H. Sakurai, et al., J. Phys. Conf. Ser. 65 (2007) 012020.
[8] F. Piuz, Nucl. Instr. and Meth. A 502 (2004) 334.
[9] A. Di Mauro, Nucl. Instr. and Meth. A 525 (2004) 334.
[10] T. Francke, V. Peskov, Nucl. Instr. and Meth. A 525 (2004) 1.
[11] F. Sauli, Nucl. Instr. and Meth. A 386 (1997) 531.
[12] H. Sakurai, et al., Nucl. Instr. and Meth. A 374 (1996) 341.
[13] A. Breskin, et al., Nucl. Instr. and Meth. A 478 (2002) 225.
[14] Y. Giomataris, Nucl. Instr. and Meth. A 376 (1996) 84.
[15] J. Va'vra, T. Sumiyoshi, Nucl. Instr. and Meth. A 553 (2005) 76.
[16] D. Mörmann, et al., Nucl. Instr. and Meth. A 504 (2003) 93.
[17] F. Tokanai, et al., Nucl. Instr. and Meth. A 571 (2007) 289.

Nuclear Instruments and Methods in Physics Research A 610 (2009) 169–173

Contents lists available at ScienceDirect

Nuclear Instruments and Methods in Physics Research A

journal homepage: www.elsevier.com/locate/nima

ogress in the development of photosensitive GEMs with resistive electrodes anufactured by a screen printing technology

Peskov [a,b,*], P. Martinengo [a], E. Nappi [a,c], R. Oliveira [a], G. Paic [b], F. Pietropaolo [d], P. Picchi [e]

Div., CERN, Geneva-23, CH-1211, Switzerland
st. de Ciencias Nucleares UNAM, Mexico
FN Bari, Bari, Italy
FN Padova, Padova, Italy
FN Frascati, Frascati, Italy

RTICLE INFO

ilable online 21 May 2009

words:
M
GEM
THGEM
photocathode
otosensitive gaseous detectors
H

ABSTRACT

An innovative photosensitive gaseous detector, consisting of a GEM-like amplification structure with double-layered electrodes (instead of commonly used metallic ones) coated with a CsI reflective photocathode, is described. In one of our latest designs, the inner electrode consists of a metallic grid and the outer one is made of resistive strips; the latter are manufactured by a screen-printing technology on the top of the metallic strips's grid The inner metallic grid is used for 2-D position measurements whereas the resistive layer provides an efficient spark-protected operation at high gains close to the breakdown limit. Detectors with active areas of 10×10 and $10 \times 20\,cm^2$ were tested under various conditions including the operation in photosensitive gas mixtures containing ethylferrocene or TMAE vapors.

The new technique could have many applications requiring robust and reliable large-area detectors for UV visualization, as for example, in Cherenkov imaging devices.

Introduction

The development of hole-type gaseous photodetectors, (e.g. pillary plates [1,2], GEM [3], THGEM [4,5]), combined with solid otocathodes sensitive to UV and even to visible light have been ccessfully perused by several groups (see for example review pers [3,6] and references therein). These detectors are proven to very promising. The main advantage of gaseous detectors erating at atmospheric pressure is the possibility to build large nsitive area (many m^2) systems since there are no serious echanical constrains on the optical-window size. Such large-ea photon detectors are attractive for some applications, for ample in Cherenkov imaging devices.

In contrast to traditional gas amplification structures, such as rallel-plate or wire type, the hole-type detectors, due to their ometric features, have strong photon-feedback suppression and, some cases, good ion feedback reduction (see [7] and references erein); both are essential for reaching high gas-gains with tectors operating with photocathodes [8]. It is important to scade a few hole-type structures (several elements operating in ndem), as to reach sufficient gains for efficient single-photon detection. These features allow the photosensitive hole-type structures to reach gas gains of $\geq 10^5$.

However, there is a fundamental problem associated with single-photoelectron detection at such high gas gains: the maximum achievable gains A_{mr} of bare hole-type structures (without photocathodes) are governed by the so-called Raether limit [9]

$$A_{mr} n_0 = Q_{max} = 10^6 - 10^7 \text{ electrons}, \quad (1)$$

where n_0 is the number of primary electrons created in the charge-collection region of the detector and Q_{max} is the critical total charge in the avalanche at which the avalanche diverges into a streamer and later, to a discharge.

Therefore, at gas gains $\geq 10^5$, any highly-ionizing radioactive background, natural or produced in high-energy physics experiments, if yielding more than 100 primary electrons (e.g. induced by heavily ionizing particles, neutron-interactions, showers and in some cases even minimum ionizing particles) will trigger occasional discharges. The precise value of Q_{max} depends on the detector's geometry and the gas composition, for example Q_{max} is larger in cascaded detectors (due to avalanche-electron diffusion [10]).

When the hole-type structure is combined with photocathodes, the maximum achievable gain A_{mf} can be additionally restricted by the feedback mechanism (see [8] for details) so that

$$A_{mf} \gamma k = 1, \quad (2)$$

* Corresponding author at: PH Div., CERN, Geneva-23, CH-1211, Switzerland. Tel.: 12 276 74 643; fax: +412 276 79 480.
E-mail address: vladimir.peskov@cern.ch (V. Peskov).

68-9002/$ - see front matter © 2009 Elsevier B.V. All rights reserved.
i:10.1016/j.nima.2009.05.070

where γ is the probability of secondary effects (which depends on electric field on the cathode surface and on the gas [8] and k is a coefficient determining what fraction of ions (in the case of the ion feedback) or photons (in the case of the photoeffect) reaches the cathode of the hole-type detector (in the case of wire-type or parallel-type detector usually $k\sim1$). Note that very often, particularly in the case of photocathodes sensitive to visible light $A_{mf}<A_{mr}$ [7].

Another drawback raises in case of applications for single-photoelectron detection, where one has to operate the detector at exceptionally high gains, hence at high voltages, entailing that any hole imperfections (tips, dust, dirt) often trigger breakdowns even before reaching the Raether limit [9].

There exists some standard procedures for limiting the destructive power of the discharges in gaseous detectors. For example, in the case of GEMs, it is recommended to segment the electrodes into several independently powered areas and to use protective diodes in the front-end electronics. However, the implementation of these, in the case of large-area devices, e.g. in RICH detectors with sensitive surfaces of several m^2, becomes rather complicated and indeed does not guarantee full reliability in long-term exploitation.

To address this problem, we have recently developed what we called a Resistive Electrode Thick GEM (RETHGEM) with electrodes made of resistive materials (instead of traditional metallic ones) [11]. The unique property of this detector is that it operates at the same time like a GEM (it can be exploited in a cascaded mode, can operate in badly quenched gases and so on) and like an avalanche resistive-plate chamber (RPC) [12], because it is fully spark-protected. Preliminary tests showed that resistive electrodes can be coated with CsI photosensitive layers and that such detectors may have rather high quantum efficiencies (QE) in the UV range, for example QE ~12.2% was measured at 185 nm in Ne [11].

The technology described in [11,13] enabled to build only small RETHGEMs, with an active area of $3\times3\,cm^2$; these early designs had rather large dead-zones (to avoid surface streamers (see [13] for explanations).

To overcome this technical problem, we recently proposed a new design of the RETHGEM with double-layered electrodes: an inner layer consisting of metallic grid or a mesh pattern and the outer one being made of either a uniform or segmented resistive material manufactured by a screen-printing technology [13]. In the latter case, each two neighboring metallic strips were coated with one common resistive strip. This new approach opens the possibility to build large-area RETHGEMs; prototypes with active areas of 5×5 and $10\times10\,cm^2$ were manufactured and successfully tested with alpha particles and X-rays [13]. This new design also offers better counting-rate characteristics [13].

For the first time, we have studied the feasibility to operate a double-layered RETHGEM as a photodetector. The cathodes were either coated with CsI photocathodes or bare-RETHGEMs were investigated in photosensitive gases.

The main focus in these studies has been on the advanced design of the double-layered photosensitive RETHGEM in which each individual metallic strip was coated by its own resistive strip. We call this device strip-RETHGEM or S-RETHGEM. As will be shown below, after optimization of some parameters such as the drift voltage and the gas composition, the S-RETHGEM was able to operate at ten times higher gains than reported earlier in [13]; this allowed not only to detect single photoelectrons with high efficiency but also to perform 2-D position measurements with UV light.

2. Detector designs and the experimental setup

Two designs of photosensitive S-RETHGEMs have been tested in this study: one with strips only on one side of the G-10 plate and the other with strips on both sides. In the latter case, the strips on one surface of the G-10 are perpendicular to the ones on the opposite face.

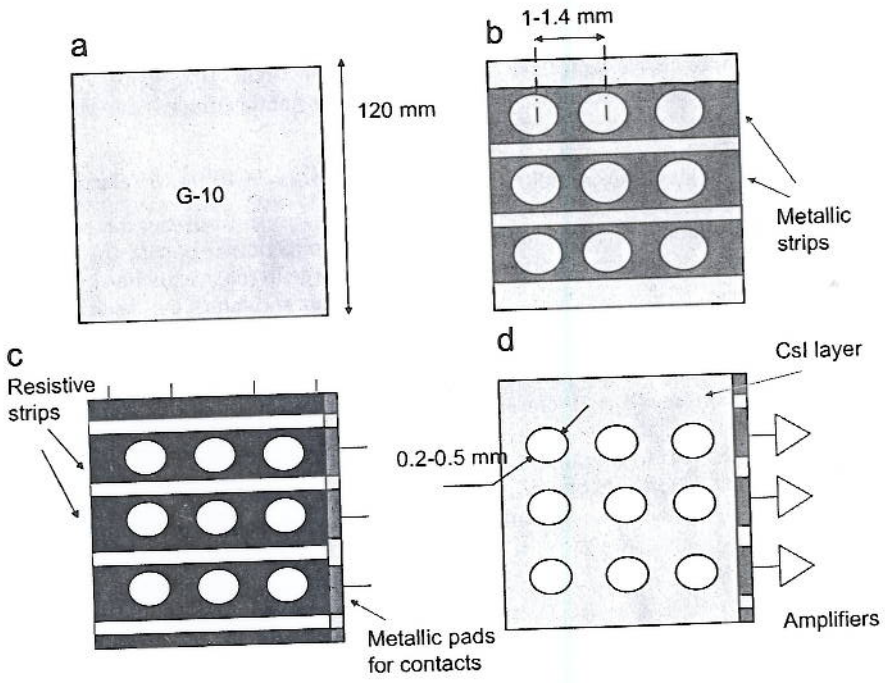

Fig. 1. Steps in the photosensitive S-RETHGEM manufacturing process: (a) bare G-10 plate, (b) metallic strips with circle opening are manufactured on the G-10 plate by a photolithographic technology, (c) resistive strips are manufactured on the top of metallic strips by a screen printing technique and holes are drilled across and (d) the top surface of the S-RETHGEM is coated with a CsI layer.

Fig. 1 schematically shows how the S-RETHGEM is manufactured. First, on the side of the bare G-10 plate (Fig. 1a) Cu strips with circular dielectric opening (Fig. 1b) were manufactured by a photolithographic technology. The width of the strips, depending on the particular design was 0.7–1 mm, their pitch was 1–1.4 mm and the circle diameter was 0.5–0.8 mm, respectively. Subsequently, the surface of each metallic strip was coated by a screen-printing technology with a 15-μm-thick resistive layer, forming the resistive strips (Fig. 1c); the gap-width between neighboring resistive strips was 0.1 mm. These double-layered plates were then cured in the oven at temperatures of 200 °C followed by holes drilling with a CNC machine-in the middle of each circle opening. Their diameter, depending on the particular design, was in the range of 0.2–0.5 mm. Note that it was very essential to keep the diameter of the drilled holes smaller than the diameter of the uncoated by Cu circles/opening on the metallic strips. This feature provided an efficient spark-protection. S-RETHGEMs with active areas of 10×10 and $10 \times 20\,cm^2$ have been manufactured following this technique. Finally, the cathode of each S-RETHGEM was coated with a 0.35-μm-thick CsI layer (Fig. 1d).

The inner metallic strips have been used to collect the charge produced by avalanches in holes situated inside each strip. The resistive grid made the detector intrinsically spark protected: in the case of sparks, the resistive layer strongly restricted the current and thus the destructive power.

The experimental setup for the RETHGEM studies is shown in Fig. 2. It consisted of a gas chamber housing a single S-RETHGEM or two S-RETHGEMs operated in cascade, an Ar(Hg) UV lamp (in some measurements a pulse D_2 lamp also was used), a monochromator, a lens focusing the light from the lamp to the input slit of the monochromator or directly to the top RETHGEM surface (for position-resolution measurements) and a gas system allowing to flush various gases (He, Ne, Ar or mixture of these with various quenchers including photosensitive vapors: ethylferrocene (EF) or TMAE [8]). For these tests we used rather pure He and Ne (9.9999%), however, we did not have the possibility to control the quality of these gases inside the detector's gas chamber.

In some control measurements, the ionization inside the gas has been produced by 5.9 keV photons from a ^{55}Fe source.

The gain measurements have been performed by two methods: photocurrent measurements (see [14] for details) or measuring the mean value of the pulse amplitudes produced by avalanches with a calibrated charge-sensitive preamplifier [15]. In both cases all metallic strips have been electrically interconnected to the picoampermeter or to the charge-sensitive amplifier, respectively.

In the case of position measurements, several charge sensitive preamplifiers have been connected to the central strips (on which the light of the Hg lamp was focused) whereas the adjacent strips have been grounded via 10 MΩ resistors.

The procedure adopted for the quantum efficiency measurements is the same as described in [16].

3. Results

Fig. 3 shows gain vs. voltage curves measured with a single and cascaded S-RETHGEMs in current mode for gains $<10^4$ and in current and pulse mode at gains $>10^4$ in various gases and for two polarities of the electric field in the drift region: a negative one $E_{dr} = -250$ V/cm and a positive one (inversed polarity) $E_{dr} = +250$ V/cm. The inversion of the electric field in the drift region allows to suppress the contribution of the natural radioactivity and additionally to increase the maximum achievable gains (see the introduction and Eq. (1)). Note that the reversed-field method has been already successfully implemented in cascaded-GEM photon detectors with reflective CsI photocathodes, to suppress charged-particle background in high energy physics experiments [17,18].

From Fig. 3 one can see that at every polarity of the electric field in the drift region, the gas gains achieved in He- and Ne-

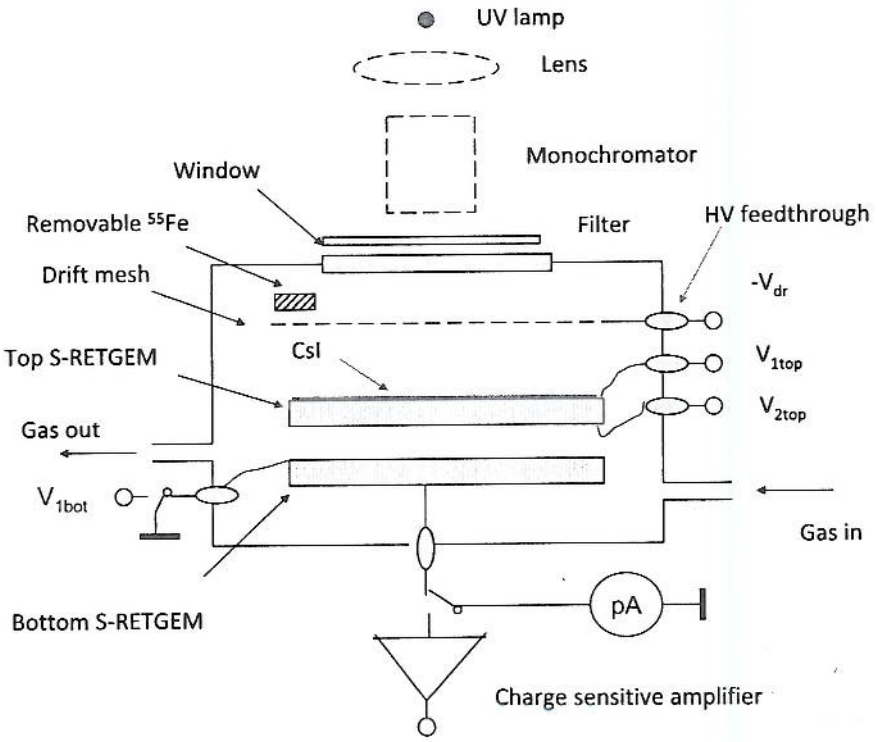

Fig. 2. A schematic drawing of the experimental set up for measuring gain, position resolution and the QE of the S-RETHGEM.

based mixtures are an order of magnitude higher than in Ar-based gases. Moreover, in He- and Ne-based gases the S-RETHGEM could operate at 10–20 fold higher gains than in the case of $E_{dr} = -250$ V/cm reaching values of 10^5 and 10^6 with a single and double S-RETHGEM, respectively. Such high gains allowed detecting single photoelectrons even with one S-RETHGEM.

Note that in Ar-based mixtures the operational voltages were considerably higher than in He- and Ne-based gas mixtures. Thus one can speculate that breakdown in the Ar-based mixture is mainly triggered by the hole imperfections (whereas in He- and Ne-filled detectors one of the conditions reflecting in formulas (1) and (2) are reached).

Note that due to the low strip capacity and the protective resistive coating, the discharges happening at gains $>10^5$–10^6 were rather weak; their energy was almost 10 fold lower than in the case of the ordinary RETHGEMs.

Gain measurements in a pulse-mode (performed at gains $>10^3$ with ^{55}Fe and at gains $>10^5$ with the UV light) yielded values typically 1.5–2 times higher than in the current mode. We attributed this difference mainly to the charging up effect [14]. Indeed, if the chamber operated in a pulse-mode continuously for 1–2 h the difference in gain measurements was reduced to 30–50%.

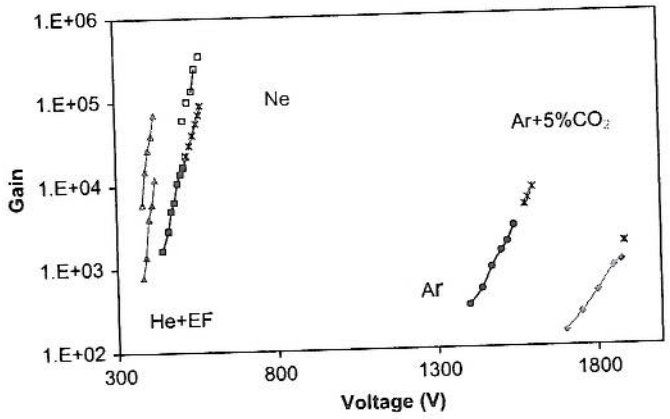

Fig. 3. Gain vs. Voltage curves measured in different configurations [single S-RETHGEM (solid symbol), double S-RETHGEM (open symbol) and inverted drift field (red asterisks)], with various gases [He+EF (triangle), Ne (square), Ar (circle), Ar+5%CO_2 (rhombus)].(For interpretation of the references to colour in this figure legend, the reader is referred to the web version of this article).

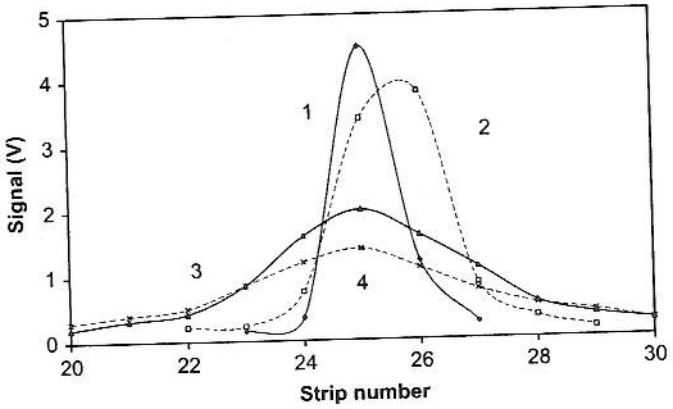

Fig. 4. Mean signal amplitude vs. strip number measurements at different conditions. The curves #1, #2 are obtained with single S-RETHGEM, #1(rhombus) when middle of the strip #25 being irradiated by the UV-light, whereas #2 (open squares), when the region between strips #25 and 26 being irradiated. The curves #3, #4 are obtained with double S-RETHGEM and with the middle of the top strip #25 being irradiated, #3 (triangles) shows the signals from the cathode strips of the bottom S-RETHGEM and #4 (stars) the signals from its anode strips.

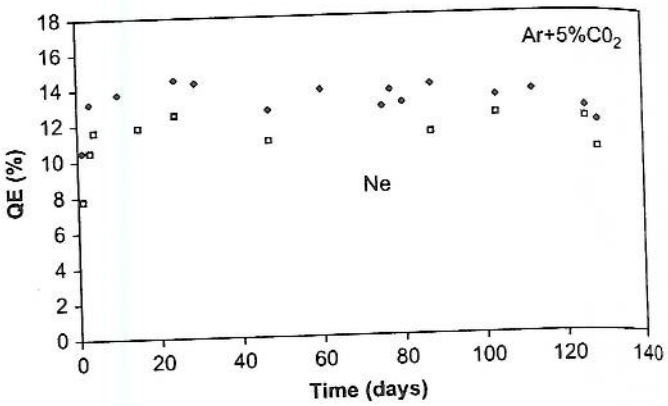

Fig. 5. QE vs. time measured in Ar+5%CO_2 (rhombus) and Ne (squares) at 1 atm. The Ar (Hg) lamp was kept on and the HV was applied to the detector only during the measurements.

Fig. 4 shows the results of the 1-D and 2-D position-resolution measurements performed with single and double S-RETHGEMs. As was mentioned above, in these measurements the UV light from the lamp has been focused on the top electrode of the S-RETHGEM (the diameter of the light spot on the cathode surface was ~0.3 mm) and the avalanche-induced signals have been simultaneously measured from the irradiated strips as well as from several neighboring strips. As one can see from the curves presented in Fig. 4, high-amplitude signals have been measured only from the irradiated strips indicating that a position resolution of about double strip pitch (~2 mm) has been achieved with the single S-RETHGEM and a few times worse (due to the hole misalignment between top and bottom S-RETHGEMs and the diffusion effect) with double S-RETHGEM. One can expect that a better position resolution could be achieved with the S-RETHGEM design having a smaller pitch of holes/strips. For comparison mention that in [19] a position resolution of 0.7 mm FWHM was achieved with double-THGEM irradiated by X-rays and having a separate resistive anode plate (the operation was with electron extraction from THGEM) followed by readout strips of 2 mm pitch.

Among several tested S-RETHGEMs, one has experienced some very mild discharges in Ar+5%CO_2 mixture at rather low gains ~10^2. By identifying the strips at which the discharges occurred and applying a −200 V negative voltage on these strips (thus lowering the voltage across the S-RETHGEM in the troubled region), we have been able to operate the remaining surface of the detector at "nominal" gas gains, as shown in Fig. 3. We consider this experience as a possible practical method to operate detectors at high gains even if several holes show defects.

The QE of the CsI coated S-RETHGEM has been measured at 185 nm (see [16] for details); it resulted to be ~12% in Ne and ~14% in Ar+10%CO_2.

Fig. 5 shows the results of monitoring the QE stability over a period of four months; as one can see from these plots, practically no degradation of the QE has been observed over this period of time. Similar stability was measured with ALICE wire-chamber CsI photon detectors [20].

In the case of EF and TMAE vapors the S-RETHGEM's sensitivity to the UV light (the S-RETHGEM operated in He-based mixtures grew almost linearly with the width of the drift gap D_r. At $D_r = 5$ cm the QE was ~1% and ~30% for EF and TMAE; in both cases the detector and the gas system were kept at 27 °C. The

noticeable difference in the QE is mainly attributed to the very different vapor pressures of EF and TMAE at 27 °C [21,22].

4. Discussion and conclusions

In this study, for the first time we have tested photosensitive RETHGEMs having double layered strip-electrode structures. This approach allows building large-area detectors. Additionally, the strip geometry offers a very safe operation (small individual strip's capacity and the resistive coatings makes discharges very mild) and the possibility to perform 2-D position measurements. Moreover, in the case of persisting discharges in some particular holes, the strip on which these holes are located could be electrically "disabled" allowing the remaining detector surface to operate at high gas gains.

We have discovered that in He- and Ne- based gas mixtures and in the case of an inverted drift field, S-RETHGEM can be operated at very high gains almost approaching the Raether limit; this allows detecting single photoelectrons even with a single S-RETHGEM.

The QE of the S-RETHGEMs is sufficiently high for many applications. For example, we are considering using CsI-coated S-RETHGEMs in the upgrade of the ALICE RICH detectors, called VHMPIDs [23]. As was shown in [13] the S-RETHGEM can operate stably at counting rates $<400\,Hz/cm^2$, namely at the expected VHPMPID counting rates of the VHMPID detector at ALICE experiment [24]. Another application on which we are working on is an early warning in case of forest fires; to this aim we are testing S-RETHGEMs operating in He+EF gas mixture, which allows to detect small flames even in the presence of direct sunlight (see [25] for details).

Acknowledgements

We thank Amos Breskin for discussions and Miranda Van Stenis for her help throughout this activity. Guy Paic acknowledges the support of the UNAM-DGAPA project IN115808.

References

[1] V. Peskov, et al., Nucl. Instr. and Meth. A 433 (1999) 492.
[2] F. Tokanai, Report at this conference.
[3] R. Chechik, et al., arXiv:0807.2086, 2008.
[4] L. Periale, et al., Nucl. Instr. and Meth. A 478 (2002) 377.
[5] R. Chechik, et al., Nucl. Instr. and Meth. A 553 (2005) 35.
[6] T. Francke, et al., IEEE Trans. Nucl. Sci. NS-49 (2002) 977.
[7] A. Lyashenko, et al., arXiv:0804.4396, 2008.
[8] T. Francke, et al., Nucl. Instr. and Meth. A 525 (2004) 1.
[9] V. Peskov, et al., IEEE Trans. Nucl. Sci. NS-48 (2001) 1070.
[10] P. Fonte, et al., Nucl. Instr. and Meth. A 416 (1998) 23.
[11] A. Di Mauro, et al., Nucl. Instr. and Meth. A 581 (2007) 225.
[12] D.F. Anderson, et al., Nucl. Instr. and Meth. A 348 (1994) 324.
[13] P. Fonte, et al., preprint arXiv:0805.2728, 2008.
[14] G. Charpak, et al., IEEE Trans. Nucl. Sci. NS-55 (2008) 1657.
[15] V. Peskov, et al., IEEE Trans. Nucl. Sci. NS-54 (2007) 1784.
[16] A. Agocs, et al., preprint arXiv:0712.2179, 2007.
[17] D. Mörmann, et al., Nucl. Instr. and Meth. A 530 (2004) 258.
[18] S. Milov, et al., J. Phys. G: Nucl. Part. Phys. 34 (2007) S701.
[19] M. Cortesi, et al., JINST 2 P09002, 2007.
[20] F. Piuz, et al., Nucl. Instr. and Meth. A 433 (1999) 178.
[21] V. Peskov, et al., Nucl. Instr. and Meth. A 283 (1989) 786.
[22] D.F. Anderson, Nucl. Instr. and Meth. A 270 (1988) 416.
[23] G. Paic, Report at ALICE Physics forum "Very high momentum identification at ALICE—a possibility" ⟨http://indico.cern.ch/conferenceDisplay.py?confId=26371⟩.
[24] J. Volpe, private communication.
[25] J.-M. Bidault, et al., Nucl. Instr. and Meth. A 580 (2007) 1036.

Nuclear Instruments and Methods in Physics Research A 610 (2009) 174–177

Contents lists available at ScienceDirect

Nuclear Instruments and Methods in Physics Research A

journal homepage: www.elsevier.com/locate/nima

The quest for a third generation of gaseous photon detectors for Cherenkov imaging counters

M. Alexeev [a,1], R. Birsa [k], F. Bradamante [j], A. Bressan [j], M. Chiosso [h], P. Ciliberti [j], G. Croci [c], M.L. Colantoni [i], S. Dalla Torre [k], S. Duarte Pinto [c], O. Denisov [i], V. Diaz [k], V. Duic [j], A. Ferrero [h], M. Finger [f], M. Finger Jr. [f], H. Fischer [d], G. Giacomini [b], M. Giorgi [j], B. Gobbo [k], R. Hagemann [d], F.H. Heinsius [d], F. Herrmann [d], K. Königsmann [d], D. Kramer [e], L. Lauser [d], S. Levorato [j], A. Maggiora [i], A. Martin [j], G. Menon [k], A. Mutter [d], F. Nerling [d], D. Panzieri [a], G. Pesaro [j], J. Polak [e,k], E. Rocco [h], L. Ropeleswki [c], F. Sauli [g], G. Sbrizzai [j], P. Schiavon [j], C. Schill [d], S. Schopferer [d], M. Slunecka [f], F. Sozzi [j], L. Steiger [e], M. Sulc [e], S. Takekawa [j], F. Tessarotto [k,*], H. Wollny [d]

[a] INFN, Sezione di Torino and University of East Piemonte, Alessandria, Italy
[b] INFN, Sezione di Trieste and University of Bari, Bari, Italy
[c] CERN, European Organization for Nuclear Research, Geneva, Switzerland
[d] Universität Freiburg, Physikalisches Institut, Freiburg, Germany
[e] Technical University of Liberec, Liberec, Czech Republic
[f] Charles University, Prague, Czech Republic and JINR, Dubna, Russia
[g] TERA Foundation, Novara, Italy
[h] INFN, Sezione di Torino and University of Torino, Torino, Italy
[i] INFN, Sezione di Torino, Torino, Italy
[j] INFN, Sezione di Trieste and University of Trieste, Trieste, Italy
[k] INFN, Sezione di Trieste, Trieste, Italy

ARTICLE INFO

Available online 27 May 2009

Keywords:
COMPASS
RICH
Photon detection
Thick GEM
CsI photoconverter

ABSTRACT

RICH (Ring Imaging CHerenkov) counters for PID in the high momentum domain and in large acceptance experiments require photon detectors covering extended surface (several square meters) and able to accept Cherenkov photons in a wide angular range. An ideal approach is represented by gaseous photon detectors, which allow covering wide surfaces at affordable costs.

The first generation of these detectors was based on the use of organic vapors. The second generation consists of CsI photocathodes and open geometry gaseous detectors (MWPC). In spite of the success of this approach, some limits of the technique arise from the bombardment of the photocathodes by the ions generated in the amplification process and by the photon feedback. A third generation of gaseous photon detectors using closed geometry, as those possible with multistage arrangements of micropattern gaseous detectors, can overcome the observed limitations.

We have started an R&D programme to develop a Thick-GEM-based photon detector and we report about our initial studies.

1. Introduction

The photon detectors used so far in Ring Imaging CHerenkov (RICH) counters are vacuum-based ones, namely photomultiplier tubes in standard or hybrid version, or gaseous detectors coupled to photon converters. The latter ones allow to cover wide surfaces at affordable costs and, thanks to their reduced material budget, they can be placed in the apparatus acceptance region.

The development of the first generation of these detectors, in which photoconverting vapors were added to the detector gas mixture, has allowed to establish RICH counters as reliable tools. This is demonstrated by remarkable examples: for instance, the RICH detectors of the E605 [1], DELPHI [2], OMEGA [3] and SLD [4] experiments. This approach requires a long conversion region, when TMAE (Tetrakis Dimethylamine Ethylene) at room temperature is used, or heated photon detectors, when the gaseous detectors with TMAE are kept at 40 °C or higher temperature, or to detect photons in the very far UV domain, below 165 nm, when

* Corresponding author.
E-mail address: fulvio.tessarotto@ts.infn.it (F. Tessarotto).
[1] On leave from JINR, Dubna, Russia

0168-9002/$ - see front matter © 2009 Elsevier B.V. All rights reserved.
doi:10.1016/j.nima.2009.05.069

the photoconverting vapor is TEA (Triethylamine). These features represent clear limitations and photoconverting vapors are being progressively abandoned; at present the only active RICH detector using photoconverting vapors is CLEO III counter [5].

The first gaseous photon detector with a solid state photoconverter has been developed within the RD26 research programme [6]: it is a MWPC where a cathode plane is a PCB segmented in pads and coated with a CsI film. These photon detectors have been selected in several experiments: NA44 [7], HADES [8], COMPASS [9], STAR [10], JLab-HallA [11], ALICE [12]. In spite of the remarkable success of proving that solid state photoconverters can operate in gaseous atmospheres, MWPCs with CsI photocathodes suffer from some performance limitations. Aging resulting in a severe decrease of the quantum efficiency is reported after a collected charge of the order of some mC/cm^2 [13]. The presence of the CsI layer causes electrical instabilities of the MWPCs accompanied by long recovery time (about 1 d) [9]: the detectors must be operated at low gain, limiting the single photoelectron detection efficiency. These features are related to the bombardment of the CsI layer by the positive ions generated in the multiplication process, that flow back to the cathode elements.

New perspectives are offered by different, more recent gaseous detector architectures: in closed geometries, as those based on a multilayer of Gas Electron Multipliers (GEMs), a good fraction of the ions is trapped in the intermediate layers, thus reducing the ion bombardment of the photocathode. The threshold Cherenkov counter Hadron Blind Detector (HBD) [14] of the Phenix experiment represents the first application of these ideas: the photon detectors are triple GEM counters operated at low total gain (about 5000). In this detector the reverse photocathode geometry effectively eliminates photon feedback from avalanches.

We are developing a large gain gaseous photon detector characterized by a closed geometry architecture and we report about the status of this R&D project.

2. The THGEM electron multiplier

THGEMs (THick GEM) [15,16] are electron multipliers derived from the GEM design, scaling the geometrical parameters and changing the production technology. The Cu-coated kapton foil of the GEM multipliers is replaced by standard PCBs and the holes are produced by mechanical drilling. The conical shape of the GEM holes that forms an uncoated polyamide ring around the hole itself is replaced by a clearance ring, the rim, surrounding the hole and obtained by Cu etching (Fig. 1). Typical values of the geometrical parameters are PCB thickness of 0.4–1 mm, hole diameter ranging between 0.3 and 1 mm, hole pitch of 0.7–1.2 mm and rim width between 0 and 0.1 mm. Large gains have been reported for detectors with single or double THGEM layers, as well as good rate capabilities [15]. THGEMs can be produced in large series and large size with standard PCB technology, they have intrinsic mechanical stiffness and are robust against damages produced by electrical discharges. On the other hand, due to the technology used, THGEM-based detectors cannot be built with very low material budget and cannot offer space resolution as pushed as GEM-based detectors.

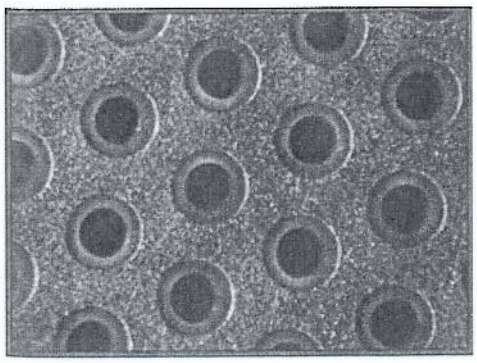

Fig. 1. Image of a THGEM with holes of 0.3 mm diameter, pitch of 0.7 mm and rim size of 0.1 mm.

These features of the THGEM-based detectors, shortly mentioned above, suggest to use them in single photon gaseous detectors; in this application, the robustness, the production technique and the mechanical characteristics are advantages, while the material budget and resolution aspects do not represent a limitation. Moreover, thanks to the reduced gaps between the multiplication stages, these detectors can be successfully used in magnetic field.

The basic architecture of a THGEM-based photon detector consists in double or triple THGEM layers, where the first layer is coated with a CsI film and acts as a reflective photocathode. This configuration is preferred to architectures with semitransparent photocathode, as it results in a larger photoconversion rate. In fact, a semitransparent photocathode requires to keep the entrance window at a fixed potential by coating it with a thin metallic film, which absorbs photons; the probability of photoelectron absorption in a reflective photocathode is lower than in a semitransparent one as the conversion probability is maximum at the entrance surface of the photoconverter.

Other possible applications of THGEM-based detectors are the active elements of sampling calorimeters and muon trackers, when large surfaces have to be instrumented and space resolution in the mm range is acceptable.

3. THGEM characterization

The first phase of our R&D activity has been dedicated to understanding the role of the various geometrical parameters of the THGEM multipliers. The study has been performed via the characterization of about 25 THGEM prototypes, inserted in single layer detectors and tested using X-ray sources.

A voltage ΔV is applied between the two THGEM faces. An electric field E_{drift} is established in the region above the so-called top THGEM face (lower potential), in order to focus the ionization electrons through the THGEM holes. It is obtained applying a potential lower than the one of the top THGEM face to a plane electrode parallel to the THGEM itself. An electric field $E_{induction}$ is applied in the region below the so-called bottom THGEM face (higher potential) to guide part of the electrons created in the multiplication process to the anode electrode, namely a conductive plane surface parallel to the THGEM PCB. In our investigation we collect the amplitude spectra of the anode signals and we measure the currents absorbed by all the electrodes (Cathode, THGEM top, THGEM bottom and anode). To perform the latter exercise, we have designed and built cheap and low consumption current meters with ~1 pA resolution, powered via batteries in order to operate at high voltage. The measurement protocols include the optimization versus gain of the E_{drift} and $E_{induction}$ values and the long term (days) measurements of the detector gain stability. Gain versus rate has also been measured for a subset of the characterized THGEMs. All the results reported below have been obtained with a gas mixture of $Ar:CO_2 = 70:30$.

The most relevant results are summarized in Figs. 2–4. The gain stability in time strongly depends on the rim size. Gain variations $\leq 20\%$ are observed when the rim is absent, while huge variations are clearly observed when the rim is large (0.1 mm)

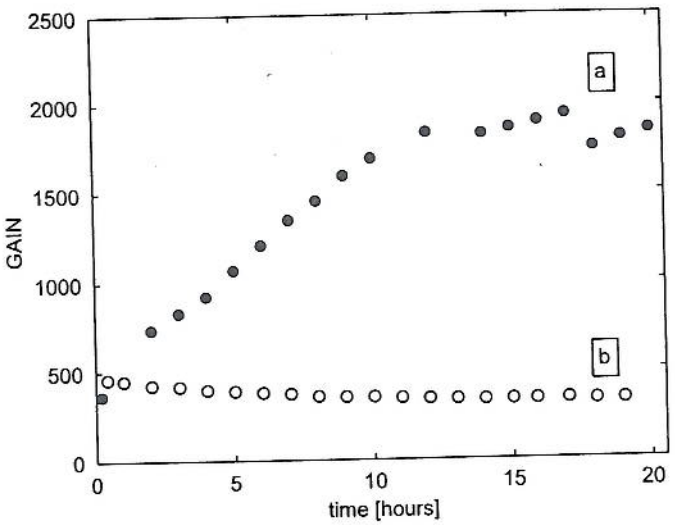

Fig. 2. Gain versus time behavior for two THGEMs with the following geometry: thickness 0.4 mm, pitch 0.8 mm and hole diameter 0.4 mm (common parameters); different parameter: 0.1 mm rim for (a), no rim for (b). Continuous detector irradiation; ΔV: 1750 V for (a) and 1330 V for (b).

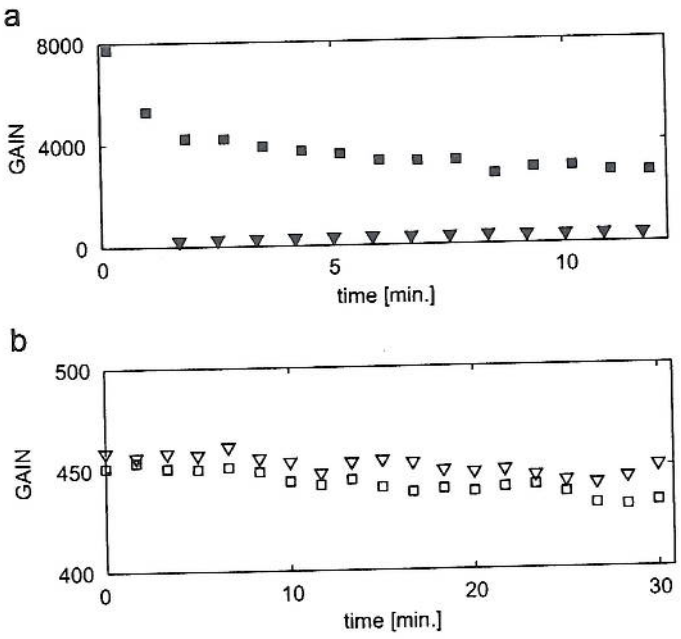

Fig. 3. Gain versus time for the THGEMs (a) and (b) described in Fig. 2. Full (empty) square points represent the gain measured irradiating the THGEM with large (no) rim after it has been for 10 h at nominal voltage without irradiation. Full (empty) triangle points represent the gain measured irradiating the THGEM with large (no) rim immediately after switching on the high voltage, after it has been switched off for 1 day.

(Fig. 2). These variations depend on the irradiation rate when the detector is powered. In Fig. 3(a) the short time gain variations of a THGEM with large rim are presented for two extreme cases: irradiating for a few minutes after the THGEM has been for 10 h at nominal voltage without irradiation, and irradiating for a few minutes at voltage switch-on after 1 day with no voltage. Large variations in the measured gain and totally different behaviors are seen. For a THGEM with no rim (Fig. 3(b)) the same measurements

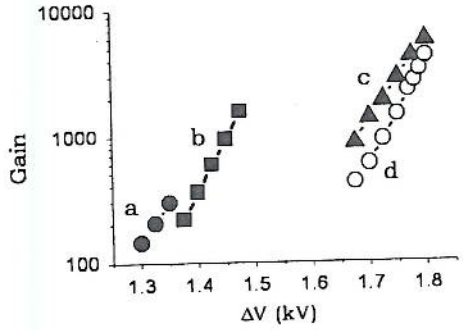

THGEM	Diam. (mm)	Pitch (mm)	Rim (mm)	Thick. (mm)
a	0.3	0.7	0	0.4
b	0.3	0.7	0.01	0.4
c	0.3	0.7	0.1	0.4
d	0.3	0.7	0	0.6

Fig. 4. Gain versus applied ΔV obtained with THGEMs of different geometry.

show on the contrary that the gain is almost independent of the previous ΔV and irradiation history.

This behavior is interpreted as caused by the displacement of charges in the PCB fiberglass plate when the high voltage is applied. This phenomenon is slow (it takes hours or days) and the resulting charge distribution is not screened in the rim region. When the detector is irradiated, the effective field causing the dielectric polarization is partially screened by the accumulation of charged particles (ions or electrons) on the free dielectric surface. The different irradiation rate thus results in different charge distribution and, consequently, in different detector gain. The huge gain variation and its dependence on the irradiation history clearly indicate that the use of large rim THGEMs must be avoided.

In Fig. 4, the maximum gain that can be obtained varying the THGEM geometrical parameters is reported. The gain increases with the rim size and with the PCB thickness. No rate dependence of the gain up to rates of at least 100 kHz/mm^2 has been observed for THGEM without rim, while gain variations versus rate are detected when a large rim is present.

4. Outlook and conclusions

Studying the characterization of a large number of THGEMs with different geometrical design, we have gained insight in the role of the various geometrical parameters.

A preliminary scheme of the device for photon detection can be derived from the outcomes of the characterization studies and the prototype production by industry. The photon detector is a chamber equipped with three or four layers of THGEM with no or reduced rim to obtain a gain above 10^5, optimizing the stability of the detector response and keeping the ion feed back at a few percent level. The upper layer is coated with a CsI film, to act as a reflective photocathode. The photons enter the chamber via a fused silica window. A PCB segmented into pads with a typical pitch of a few mm collects the signal. A digital read-out system with high sensitive front-end stage and good time resolution is coupled to the detector. The active surface of a single unit can easily be larger than $50 \times 50\,\text{cm}^2$ and the dead zone kept below 15% of the surface.

This preliminary design will be confirmed by the next studies.

We are now ready for the second phase of our R&D activity, namely to address the specific requests posed by the detection of

ingle photons. At present, this dedicated studies are starting. The utcome of our investigation obtained so far can be beneficial also o THGEM applications in different fields.

Acknowledgment

The authors are grateful to Prof. A. Breskin for his constant encouragement and many stimulating discussions.

References

[1] M. Adams, et al., Nucl. Instr. and Meth. 217 (1983) 237.
[2] E. Albrecht, Nucl. Instr. and Meth. A 433 (1999) 47 and references therein.
[3] H.-W. Siebert, et al., Nucl. Instr. and Meth. A 343 (1994) 60.
[4] J. Va'vra, Nucl. Instr. and Meth. A 433 (1999) 59.
[5] M. Artuso, et al., Nucl. Instr. and Meth. A 554 (2005) 147.
[6] The RD26 Collaboration, RD26 Status Reports: CERN/DRDC 93-36, CERN/DRDC 94-49, CERN/DRDC 96-20.
[7] C.W. Fabjan, et al., Nucl. Instr. and Meth. 367 (1995) 240; M. Spegel, Nucl. Instr. and Meth. A 433 (1999) 366.
[8] J. Friese, et al., Nucl. Instr. and Meth. A 438 (1999) 86; H. Rabus, et al., Nucl. Instr. and Meth. A 438 (1999) 94; R. Gernhäuser, et al., Nucl. Instr. and Meth. A 438 (1999) 104.
[9] E. Albrecht, et al., Nucl. Instr. and Meth. A 553 (2005) 215 and references therein.
[10] A. Braem, et al., Nucl. Instr. and Meth. A 499 (2003) 720.
[11] F. Garibaldi, et al., Nucl. Instr. and Meth. A 502 (2003) 117; M. Iodice, et al., Nucl. Instr. and Meth. A 553 (2005) 231.
[12] The ALICE Collaboration, Technical Design Report of the High Momentum Particle Identification Detector, CERN/LHCC 98-19, ALICE TDR 1, 14 August 1998.
[13] A. Braem, et al., Nucl. Instr. and Meth. A 553 (2005) 187; H. Hoedlmoser, et al., Nucl. Instr. and Meth. A 574 (2007) 28.
[14] A. Kozlov, et al., Nucl. Instr. and Meth. A 523 (2004) 345; Z. Fraenkel, et al., Nucl. Instr. and Meth. A 546 (2005) 466; A. Milov, et al., J. Phys. G: Nucl. Part. Phys. 34 (2007) S701.
[15] R. Chechik, et al., Nucl. Instr. and Meth. A 535 (2004) 303; R. Chechik, et al., Nucl. Instr. and Meth. A 553 (2005) 35; C. Shalem, et al., Nucl. Instr. and Meth. A 558 (2006) 475.
[16] J.M. Bidault, et al., Nucl. Phys. B (Proc. Suppl.) (2006) 199.